TRAJECTORY OPTIMIZATION OF EVTOL VEHICLES FOR URBAN AIR MOBILITY USING INDIRECT METHODS

Kshitij Mall¹, Rishikesh Gadre², Jonah Gerardus³ & Daniel A. DeLaurentis⁴

¹Post-Doctoral Research Associate, School of Aeronautics and Astronautics, Purdue University
 ²Undergraduate Research Assistant, School of Aeronautics and Astronautics, Purdue University
 ³Graduate Research Assistant, School of Aeronautics and Astronautics, Purdue University
 ⁴Bruce Reese Professor of Aeronautics and Astronautics, Purdue University

Abstract

Trajectory optimization of electric vertical takeoff and landing (eVTOL) vehicles for urban air mobility (UAM) missions such as passenger transportation and cargo delivery has only been sparingly studied. Tools for the rapid generation of high-quality trajectories would be useful to many UAM stakeholder organizations, including research organizations, vehicle original equipment manufacturer companies, and policy and regulation communities. Analyses enabled by such tools could accelerate progress towards the successful introduction of UAM operations. High-quality optimal cruise, descent, and landing trajectories for eVTOL vehicles under operational constraints are generated in this study using indirect methods of optimization. We believe this is the first paper to use indirect methods for trajectory optimization of eVTOL vehicles for UAM missions. For simulations, we use our model of the EHang-184 eVTOL vehicle. Three cases of the eVTOL trajectory optimization problem have been devised and solved using an advance indirect method, the Uniform Trigonometrization Method (UTM). The results generated using the UTM were compared and validated with a popular direct pseudospectral method solver, GPOPS-II. The advantages and limitations of utilizing the UTM are shared, and future work for effective resolution of these issues is listed.

Keywords: optimal control theory, urban air mobility, uniform trigonometrization method, indirect methods

1. Introduction

Urban Air Mobility (UAM) is considered a sub-category of Advanced Air Mobility (AAM) and is intended as an alternative mode of urban transportation. UAM has been proposed as a solution to ground transportation congestion for both passenger commutes, cargo, and logistic services [1]. Currently in its developmental phase, most UAM operations will rely on small-scale electric vertical take-off and landing (eVTOL) or electric short take-off and landing (eSTOL) vehicles [2]. Most UAM vehicles are currently being developed to suit flight operation policies and requirements within an urban or metropolitan airspace. UAM vehicles are expected to lower CO₂ and noise emissions and be able to operate with shorter runways or helipads within the metropolitan area [3]. Thus, the technological advancements in aircraft design allow for eVTOL and eSTOL to be the primary choice for UAM operations.

Many aspects of the UAM missions are under study by government agencies like NASA, companies like Airbus, Joby Aviation, Kitty Hawk, Lilium, Terrafugia, Uber Air, Volocopter, and EHang, and university researchers at Purdue University, Georgia Institute of Technology, et cetera [4, 5, 6, 7, 8, 9, 10, 11]. The rise in popularity and demand for UAM operations are mainly due to intense congestion and the exponential increase in CO₂ emissions. For example, Chicago suffers from the worst traffic congestion in the US, with an average driver gaining about 155 driving hours in 2022 [12]. On the other hand, there is a growing commercial interest in the cargo and logistics segment. Implementing a combination of UAM vehicles and delivery trucks shows a reduction in CO₂ emissions within the

operating network [5].

The advantages of UAM come with a cost. Similar to other new transportation innovations, multiple challenges arise, stretching the capability, operability, and feasibility of UAM operations as a mode of transport. A recent study shows potential challenges in this domain, including but not limited to safety, community acceptance, security, and the availability of supporting infrastructure [1]. Our paper focuses on addressing the challenge of optimal UAM trajectory planning. Trajectory optimization is crucial for fulfilling multiple desirable aspects of UAM operations, such as collision avoidance [13], energy savings [14], reductions in travel and commute times [15], etc. Certain eVTOL concepts have emerged using different design approaches in the literature. However, trajectory optimization of such eVTOL vehicles for cruise, descent, and landing missions in the UAM environment has received very little attention.

Trajectory optimization problems can be solved using either direct methods or indirect methods. Direct methods are more straightforward and very efficient in solving multi-phase problems with many constraints. However, these direct methods result in lower resolution results as compared to mathematically richer indirect methods for certain problems, such as singular control problems. Chattering or solutions with many jitters are obtained using direct methods that cannot be implemented in a real-world scenario. Several recent advancements in indirect methods [16, 17, 18, 19, 20, 21] have given birth to a technique known as the Uniform Trigonometrization Method (UTM), which generates higher-resolution, optimal results. Recently, it was discovered by our team that indirect methods result in a better and different solution than direct methods for certain optimal control problems (OCPs) [22]. Several other complex OCPs from different domains have been solved using the UTM [23, 24, 25, 26, 27, 28, 29, 30].

Ref. [15] shows a convex optimization approach for UAM trajectory planning to minimize the energy required for UAM vehicles using aerodynamic constraints. The authors proposed an optimization algorithm using sequential convex programming (SCP) to model the dynamic behavior and movement of UAM vehicles concerning the safety of landing multi-rotor vehicles in complex urban landscapes. In another study, direct collocation optimization methods were used to minimize battery-energy usage during take-off and landing phases involving the aerodynamic constraints of UAM vehicles. Previously, we used advance indirect methods for the trajectory planning of UAM missions requiring safe landing assurance [31]. Previous works have also explored wind-optimal lateral trajectories [32], real-time merging control of eVTOL for UAM [33], optimal vertiport airspace and approach control strategies for UAM [34], and optimal flight trajectory generation algorithms for UAM [35].

The OCP used in this study was solved in ref. [36] using convex optimization. An indirect methods-based Python toolbox, *Giuseppe*, was used to solve this problem using the UTM [18], which forms the main contribution of this paper. Three cases of the eVTOL trajectory optimization problem have been devised and presented in this study, which forms the secondary contribution of this work. For validation and comparison purposes, we used a popular direct pseudospectral method (PSM)-based solver, *GPOPS-II* [37]. The next section illustrates a mathematical form of the eVTOL trajectory optimization problem for UAM missions.

2. Optimal Control Problem Formulation

The OCP used in this study is taken verbatim from ref. [36]. The following subsection shows the details of the problem statement. The solution process using the advance indirect method is also shown.

2.1 Problem Statement

Equation (1) describes the OCP corresponding to the eVTOL cruise, descent, and landing problem.

minimize:
$$J = \int_{t_0}^{t_f} \frac{1}{2} \left(\frac{T}{T_{\text{MAX}}}\right)^2 dt$$
 (1a)

subject to:
$$\dot{x} = v_x$$
 (1b)

$$\dot{z} = v_z \tag{1c}$$

$$\dot{v}_x = \frac{T\sin\theta}{m} - \frac{D_x}{m} \tag{1d}$$

$$\dot{v}_x = \frac{T\sin\theta}{m} - \frac{D_x}{m}$$

$$\dot{v}_z = \frac{T\cos\theta}{m} - \frac{D_z}{m} - g$$
(1d)

where:
$$D_x = \frac{1}{2}\rho v_x^2 S_x C_D \tag{1f}$$

$$D_z = \frac{1}{2}\rho v_z^2 S_z C_D \tag{1g}$$

with constraints:
$$0 \le x \le x_{MAX}$$
 (1h)

$$0 \le z \le z_{\mathsf{MAX}} \tag{1i}$$

$$v = \sqrt{v_x^2 + v_z^2} \le v_{\text{MAX}} \tag{1j}$$

$$0 \le T \le T_{\mathsf{MAX}} \tag{1k}$$

In the above equations, x is the along-track distance; z is the altitude; v_x is the horizontal velocity; v_z is the vertical component of the airspeed; S_x is the horizontal reference area of the vehicle; S_z is the vertical reference area of the vehicle; ρ is the atmospheric density of Earth; D_x is the horizontal drag force; D_z is the vertical drag force; T is the net thrust generated; θ is the rotor tip-path-plane pitch angle; m is the mass of the vehicle, and g is the gravitational acceleration.

2.2 Chosen Electric Vertical Takeoff and Landing Vehicle

UAM companies are racing to develop and release their vehicles for the market. Currently, the UAM sector is rapidly advancing alongside technological innovations, with several key companies leading the market. Joby Aviation is progressing towards obtaining an FAA certification, allowing it to begin on-demand commercial air taxi operations by 2024 [38]. The Archer Midnight, Archer Aviation's second full-scale eVTOL aircraft, has just completed its transition flight testing [39]. The Lilium Jet is progressing through its developmental phase and is expected to start operating passenger services by 2026, connecting locations within the French Riviera [40]. The EHang-216 (EHang-184's successor) just completed its first successful passenger demonstration flight in the UAE [41].

For this study, we chose the EHang-184 as our eVTOL vehicle for running simulations due to data availability. The EHang-184 is a type of autonomous aerial vehicle (AAV) that is pilot-free and requires no direct human interaction to operate. The operating parameters and specifications for EHang-184 are specified in Table 1 and obtained from ref. [36]. However, the EHang-184 has been discontinued and replaced by its successor, the EHang-216. Note that any type of eVTOL vehicle can be easily incorporated into the methodology used in this study.



Figure 1 – The EHang-184 AAV obtained from ref. [42].

2.3 Problem Parameters and Cases

The vehicle and Earth parameters are given in Table 1. These values are taken directly from ref. [36].

Table 1 – Constants related to the eVTOL vehicle and Earth used in this study.

Parameter	Unit	Value
g	m/s ²	9.81
m	kg	240
ρ	kg/m ³	1.225
S_{X}	m^2	2.11
S_{Z}	m^2	1.47
x_{MAX}	m	20,000
z_{MAX}	m	500
T_{MAX}	N	4,800

The initial, terminal, and bounding values of the time, states, and controls are shown in Table 2. The values for time of flight and maximum velocity in this table depend on three cases designed by the authors. These three cases are described as follows.

Table 2 – Boundary and bounding conditions for the time and states of the eVTOL vehicle trajectory optimization problem [36].

Parameter	Unit	Initial Value	Final Value	Minimum Value	Maximum Value
\overline{t}	S	0	Case Dependent	0	1,500
X	m	0	20,000	0	20,000
z	m	500	0	0	500
v_x	m/s	27.78	0	Case Dependent	Case Dependent
v_z	m/s	0	0	Case Dependent	Case Dependent

In the first case, there are no path constraints, but there is a T control constraint as specified in Eq. (1k). Additionally, in the first case, the time of flight is kept free. In the second case, all conditions are similar to those in case 1, except the time of flight is kept fixed. Bounds on the maximum velocity, v_{MAX} , are introduced in the third case. The remaining conditions for the third case are the same as in the first case. Table 3 summarizes the three cases designed for this study. The next section shows a detailed approach to solving this problem using the UTM.

Table 3 – Specifications for the three cases considered in this study.

	Final Time (t_f)	Maximum Velocity (VMAX)
Case 1	Free	Free
Case 2	1500 s	Free
Case 3	Free	30 m/s

3. Solution Process Using the Uniform Trigonometrization Method

While using the UTM, we first need to transform controls that have bounds. Implicit bounds are placed on control T by using a trigonometric substitution through the UTM. The other control, θ , was left unconstrained for this study.

$$T = 2400(1 + \sin T_{TRIG}) \tag{2}$$

The second step in the UTM is to impose path constraints using a penalty function of secant form. Only for case 3, there is a path constraint on the velocity as specified in Eq. (1j). Using the problem statement given in Eq. (1), the Hamiltonian can be formulated as

$$H = \lambda_x v_x + \lambda_z v_z + \frac{\lambda_{v_x}}{m} \left(2400(1 + \sin(T_{TRIG})) \sin(\theta) - \frac{1}{2} \rho v_x^2 S_x C_D \right)$$

$$+ \frac{\lambda_{v_z}}{m} \left(2400(1 + \sin(T_{TRIG})) \cos(\theta) - \frac{1}{2} \rho v_z^2 S_z C_D \right] - mg \right) + \varepsilon_v \sec\left(\frac{\pi}{2} v_{\mathsf{EXPR}}\right)$$
(3)

where ε_v is an error parameter to impose the maximum velocity constraint and v_{EXPR} is $\frac{2v - v_{\text{MAX}} - v_{\text{MIN}}}{v_{\text{MAX}} - v_{\text{MIN}}}$.

When velocity reaches its extremal values, the expression $\sec\left(\frac{\pi}{2}v_{\text{EXPR}}\right)$ becomes infinitely large in magnitude. The objective functional, J, thereby gains infinitely high values, and the solution is discarded by the solver during its search for an optimal trajectory.

The optimal control laws can then be obtained using Eq. (4) and are shown in Eq. (5) and Eq. (6), where * indicates optimal solutions.

$$\frac{\partial H}{\partial u} = 0 \tag{4}$$

$$\theta^* = \operatorname{atan}\left(\frac{\lambda_{\nu_x}}{\lambda_{\nu_z}}\right) \tag{5}$$

$$T_{\mathsf{TRIG}}^* = \begin{cases} -\frac{\pi}{2} \to T_{\mathsf{MIN}} \\ \arcsin\left(-\frac{2 \ T_{\mathsf{MAX}}(\lambda_{\nu_x} \sin\theta + \lambda_{\nu_z} \cos\theta)}{m} - 1\right) \\ \frac{\pi}{2} \to T_{\mathsf{MAX}} \end{cases} \tag{6}$$

The costate equations obtained from the Hamiltonian are described in Eq. (7a) - Eq. (7d).

$$\dot{\lambda_x} = -\left[\frac{\partial H}{\partial x}\right]^T = 0 \tag{7a}$$

$$\dot{\lambda_z} = -\left[\frac{\partial H}{\partial z}\right]^T = 0 \tag{7b}$$

$$\dot{\lambda_{v_x}} = -\left[\frac{\partial H}{\partial v_x}\right]^T = -\lambda_x + \frac{\lambda_{v_x} C_D S_x \rho v_x}{m} - \frac{\varepsilon_v \pi v_x}{v_{\mathsf{MAX}} - v_{\mathsf{MIN}}} \sec\left(\frac{\pi}{2} v_{\mathsf{EXPR}}\right) \tan\left(\frac{\pi}{2} v_{\mathsf{EXPR}}\right) \tag{7c}$$

$$\dot{\lambda_{v_z}} = -\left[\frac{\partial H}{\partial v_z}\right]^T = -\lambda_z + \frac{\lambda_{v_z} C_D S_z \rho v_z}{m} - \frac{\varepsilon_v \pi v_z}{v_{\mathsf{MAX}} - v_{\mathsf{MIN}}} \sec\left(\frac{\pi}{2} v_{\mathsf{EXPR}}\right) \tan\left(\frac{\pi}{2} v_{\mathsf{EXPR}}\right) \tag{7d}$$

Along with the UTM, a standard numerical continuation approach [43, 44] has been utilized in this study. First, a simpler version of the original problem is solved. The solution obtained for this simpler problem is then used as a guess for the subsequent, more complex versions of the problem. The continuation process in a particular set is continued until the desired conditions are met. Note that the sequence and step size of the continuation sets have been found by the authors using trial and error along with engineering judgment.

Scaling was only performed on the objective function, in which T was divided by T_{MAX} . Thus, the unit of the objective functional, J, became seconds. Since some variables, like x, have high values as compared to z, scaling or normalizing these variables could possibly speed up solving this problem. Scaling or normalization of states and other parameters have been left out of this study as already rapid computation speeds were obtained.

4. Results and Discussion

A python-based optimal control solver, Giuseppe, is equipped with UTM and used to solve the three cases discussed in Section 2. Giuseppe was developed at Purdue University in the System of Systems lab. All computations were performed on an Apple M3 Pro chip with 18 GB of unified RAM. The following subsections include the results and their comparison for the three cases.

4.1 Case 1: Unconstrained with Free Time of Flight

Created primarily for validation and verification purposes, this case is the easiest to solve among the three since all parameters save for the thrust control, T, are unconstrained.

4.1.1 Continuation Process

Propagate the trajectory for 1 second using the initial conditions shown in Table 2. The guess value for each costate is chosen as 0.1. A quick convergence is obtained for this seed trajectory since it is very short and easy to solve. In the first continuation set comprising 5 steps, v_{x_f} and v_{z_f} only are varied until they reach 0 m/s. x_f , z_f , and tolerance values are then changed in 50 steps to the desired final values. The continuation process for case 1 is summarized in Table 4.

Table 4 – Continuation strategy for case 1 of the UAM trajectory optimization problem.

Continuation	(seed)	#1	#2
Steps		5	50
x_f [m]	32.66		20,000
z_f [m]	501.46		0
v_{x_f} [m/s]	36.73	0	
v_{z_f} [m/s]	1.06	0	
Solver Tolerance	10^{-4}		10^{-6}

It should be noted that due to this continuation process, more computation time is needed by the UTM to obtain the final optimal solution. Several trajectories generated through this continuation process showcase the evolution of the solution structure, thereby providing further useful insights.

4.1.2 Verification and Validation

GPOPS-II, based on pseudospectral methods (PSM), was employed in this study for verification and validation of the UTM results. The parameters used for setting up and solving this problem using GPOPS-II are shown in Table 5.

Table 5 – GPOPS-II setup parameters and their values for this study.

Parameter	Value
Solver	IPOPT
Mesh Refinement Method	hp-PattersonRao
Maximum Iterations	50
Minimum Collocation Points	3
Maximum Collocation Points	10
Mesh Refinement Tolerance	10^{-6}
Linear Solver	ma57
Derivatives Supplier	sparseCD
Derivative Level	second
Method	RPM-Differentiation

The states and control plots obtained using the UTM and PSM are shown in Fig. 2. Since the objective is to minimize the control effort, the eVTOL vehicle quickly increases its speed to 32.43 m/s. This is the maximum possible speed of the eVTOL vehicle based on the given boundary conditions. v_z needs to have negative values for the vehicle to descend. On the other hand, v_x needs to be

positive for increasing the distance x while minimizing the control effort. Near the start and end of the trajectory, quick changes in the velocities necessitate sharp jumps in the controls T and θ .

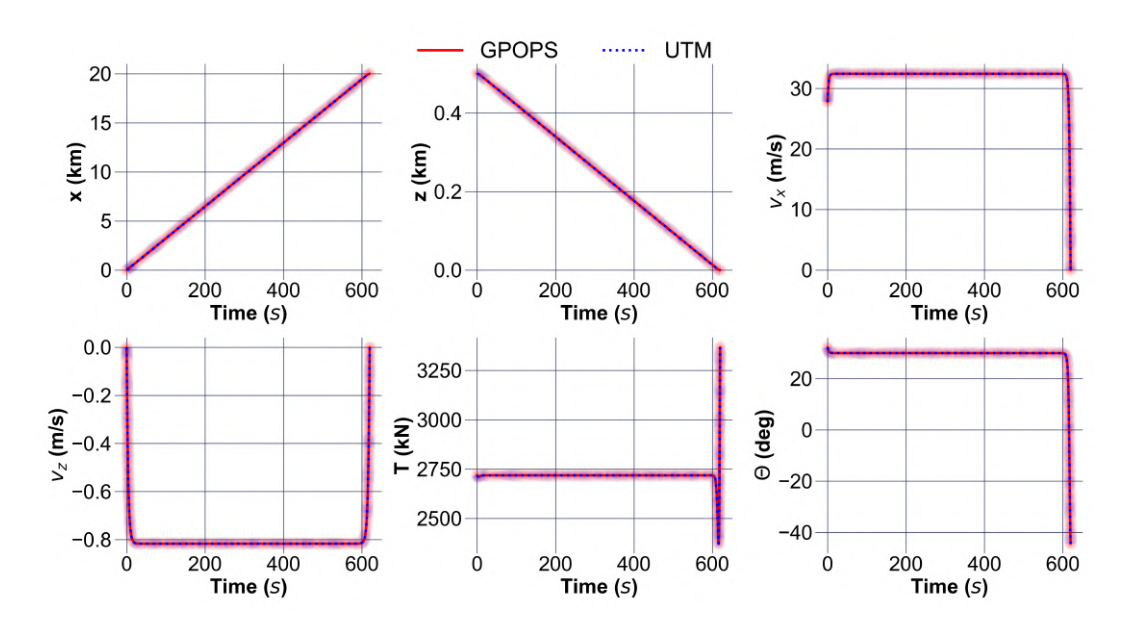


Figure 2 – Time history plots for states and controls obtained using the UTM and PSM for case 1 of this study. The results from the UTM and PSM match exactly. All the constraints are satisfied.

Thrust and pitch angle controls stay constant for a significant part of the trajectory.

The costates and Hamiltonian plots obtained using the UTM and PSM are shown in Fig. 3. In indirect methods of optimization, the costates play a crucial role in determining the optimal control values. The results obtained for case 1 using the UTM were found to be in excellent agreement with the corresponding results from PSM. Since it is a free final time problem, the Hamiltonian should be 0 based on a transversality condition [45]. Note that the PSM results for the remaining two cases have also been found to match with the corresponding UTM results. Hence, the PSM results for the remaining two cases have been excluded from this study for brevity.

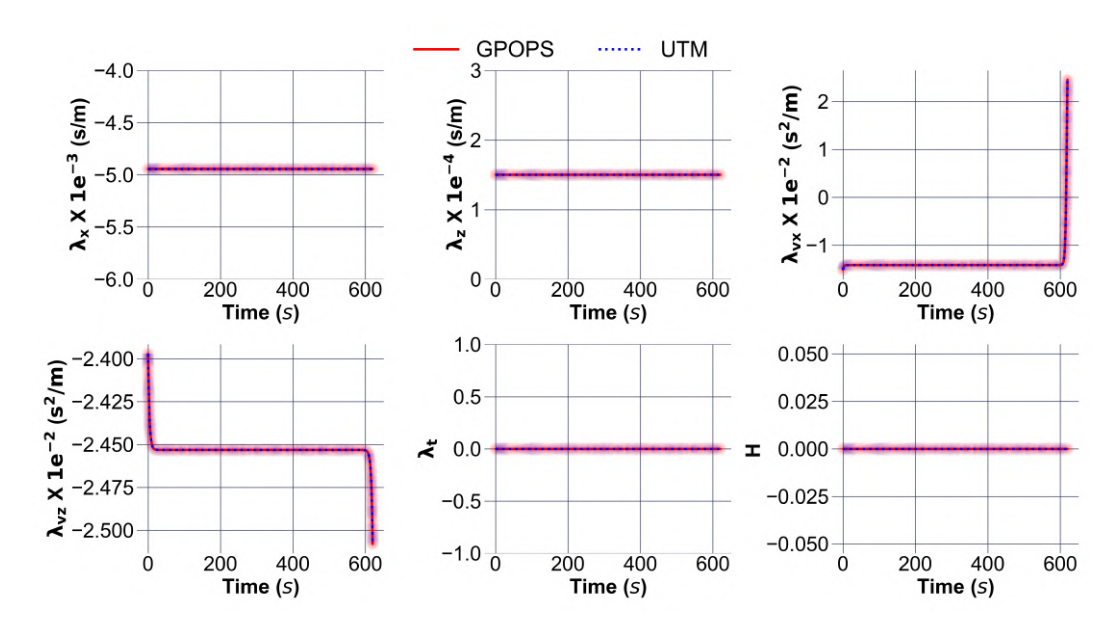


Figure 3 – Costates and Hamiltonian time history plots for Case 1 are shown here. The problem is very sensitive and hard to solve as the costates have values close to 0. Excellent agreement was found between the UTM and PSM results.

The first continuation set for case 1 is depicted graphically in Fig. 4. The solution structure drastically changes from a seed solution (shown in a red dashed line) to the final solution for this set (shown by a solid blue line). Figure 4 shows that even if the initial guess is bad and if the seed solution is obtained in an undesirable region, the continuation process can pull the trajectory back to the desired region of interest.

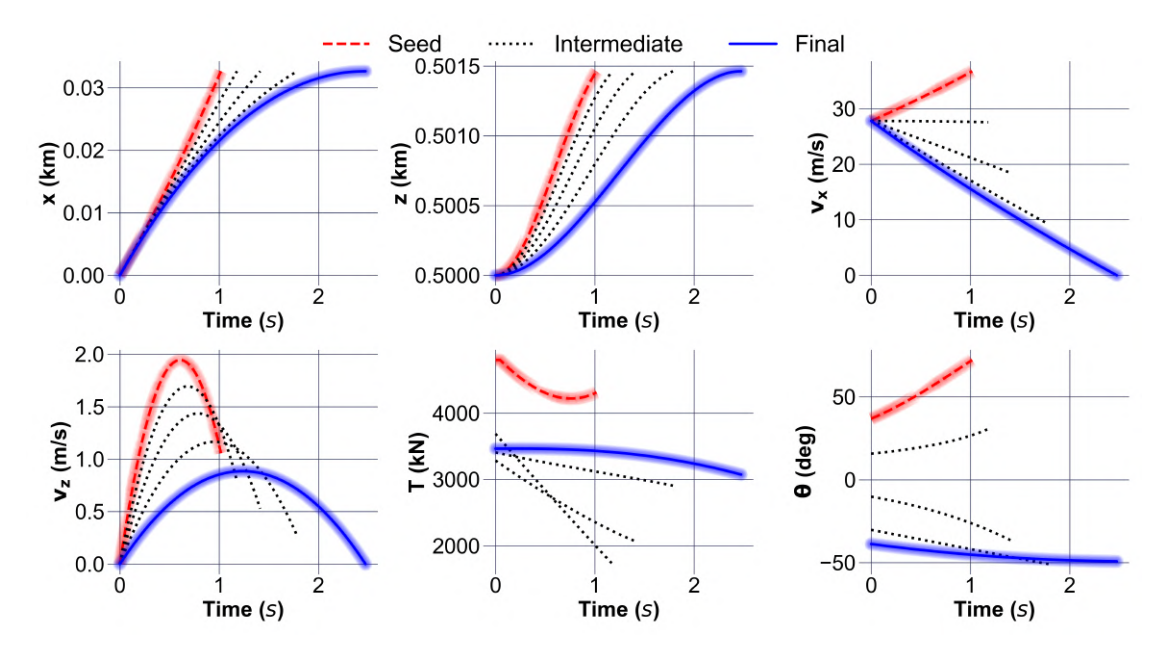


Figure 4 – Results for continuation on v_{x_f} and v_{z_f} in the first continuation set of case 1 are shown in this plot. The red dashed line is the seed solution. The intermediate results are shown in black dotted lines. The final trajectory, with a t_f of around 2.5 s, is shown in a blue solid line.

4.2 Case 2: Unconstrained with Fixed Time of Flight

This case is more difficult to solve than case 1, as the final time of flight is fixed. As a result, it is very hard to guess apriori the continuation sequence for this problem. However, continuation solutions for case 1 provide insights on setting up the continuation strategy for case 2.

4.2.1 Continuation Process

A convergence for a 1-second seed solution was successfully obtained for this case, similar to case 1. The guess value for each costate is again chosen as 0.1 to obtain this seed solution. v_{x_f} , v_{z_f} , and t_f are then varied in 50 steps until they reach values of 0, 0, and 620, respectively. The final value of t_f in this continuation step was chosen as 620 s to imitate the results of case 1. t_f , x_f , and z_f are then changed in 140 steps to the desired final values. Note that the continuation process requires more steps as this case becomes more complex and hard to solve as compared to case 1. In the third and final continuation set, the value of t_f and solver tolerance are changed to the desired values in 5 steps. The continuation process for case 2 is summarized in Table 6.

Table 6 – Continuation strategy for case 2 of the UAM trajectory optimization problem.

Continuation	(seed)	#1	#2	#3
Steps		50	140	5
t_f [s]	1	2.5	620	1,500
x_f [m]	32.66		20,000	
z_f [m]	501.46		0	
v_{x_f} [m/s]	36.72	0		
v_{z_f} [m/s]	1.06	0		
Solver Tolerance	10^{-4}			10^{-6}

4.2.2 Results Using the UTM

The time history of states and controls for this case is shown in Fig. 5. It was found that the additional constraints never became active. For instance, the values of x and z always stayed within their bounds. While case 1 had a total flight time of 620 s, case 2 was forced to have a longer flight time of 1500 s. Because of the longer time of flight, the values of the velocity components, v_x and v_z , are already within bounds and lower than those in case 1.

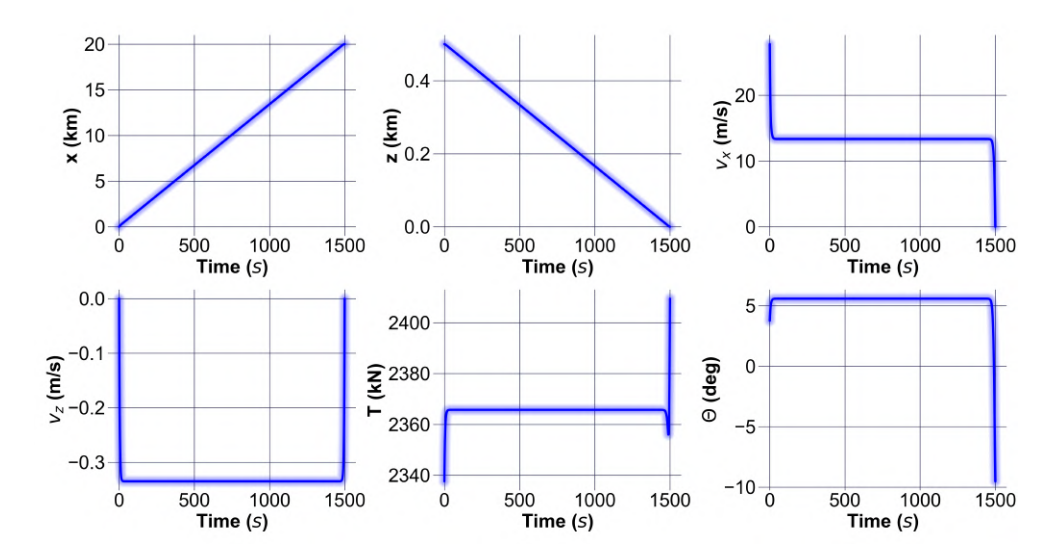


Figure 5 – States and control plots for case 2 are shown in this figure. Except for the v_x subplot, the pattern of remaining states and controls matches very closely with the results from case 1.

The final continuation set for case 2 is shown in Fig. 6. The solution structure is quite similar from the seed solution (shown in a red dashed line) to the final solution for this set (shown by a solid blue line). All the states and controls have a uniform change pattern except for v_x . For a lower t_f , v_x increases first to a high cruise speed and dips at the very end of the trajectory. However, as t_f increases, v_x changes its pattern and starts to quickly drop down to lower cruise speeds, and then further dip down to 0 m/s in the end.

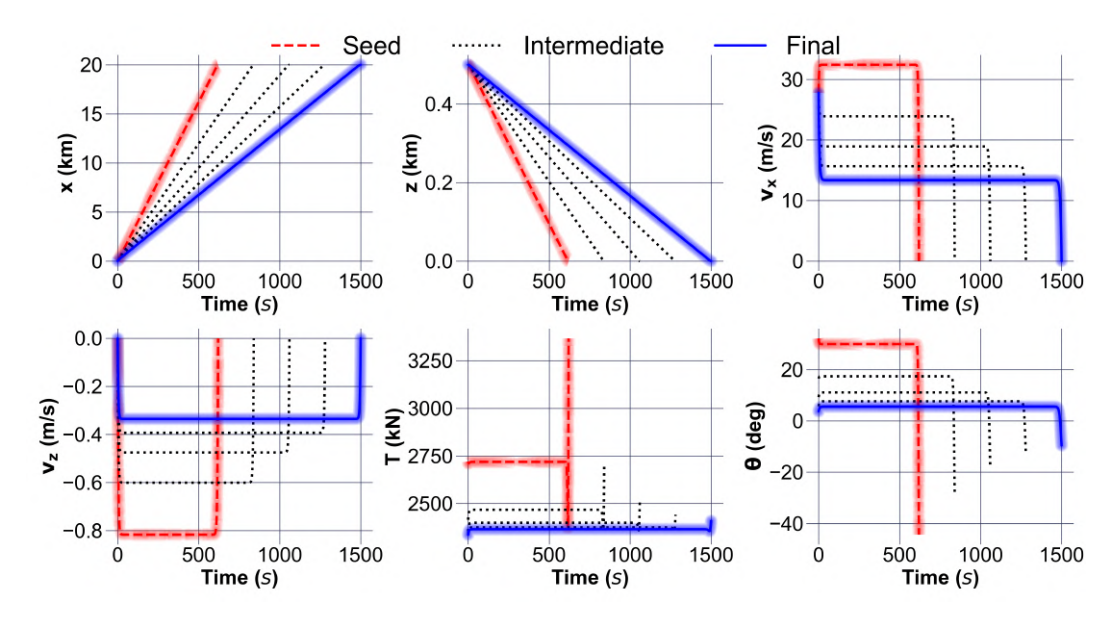


Figure 6 – The results for case 2's final continuation set on t_f are depicted in this plot. The red dashed line is a seed solution similar to case 1. The intermediate results are shown in black dotted lines with increasing values of t_f . The final trajectory, with t_f as 1500 s, is shown in a blue solid line.

4.3 Case 3: Velocity Magnitude Constraint and Free Time of Flight

This is the most complex case designed in this study. Here, the velocity constraint becomes active for a significant part (the cruise phase) of the eVTOL vehicle's trajectory. Traditional indirect methods are quite cumbersome and formidable for this case, as multiple arcs need to be developed. However, the UTM solves for a single arc and enables quick convergence by utilizing the continuation process discussed as follows.

4.3.1 Continuation Process

The continuation process for case 3 is summarized in Table 7. The continuation process for case 3 is very similar to that of case 1. An additional continuation set is required to bring down v_{MAX} from 36.73 m/s to 30 m/s in 10 steps. Similarly, two continuation sets were used to bring down the value of an error parameter ε_{ν} from 10^{-4} to 10^{-8} in 40 steps. The computation time to solve this case is high as a larger number of intermediate trajectories are generated as compared to the other two cases.

Table 7 – 0	Continuation	strategy fo	or case 3 of the	UAM trajectory	optimization	problem.

Continuation	(seed)	#1	#2	#3	#4	#5	#6
Steps		10	200	10	20	20	2
x_f [m]	32.66		20,000				
z_f [m]	501.46		0				
v_{x_f} [m/s]	36.73	0					
v_{z_f} [m/s]	1.06	0					
v_{MAX} [m/s]	40			30			
\mathcal{E}_{v}	10^{-4}				10^{-6}	10^{-8}	
Tolerance	10^{-4}						10^{-6}

4.3.2 Results Using the UTM

The time history of states and controls for this case is shown in Fig. 7. It was found that only the constraint on v is active. Since this case is forced to have a lower v_{MAX} value, the time of flight of the

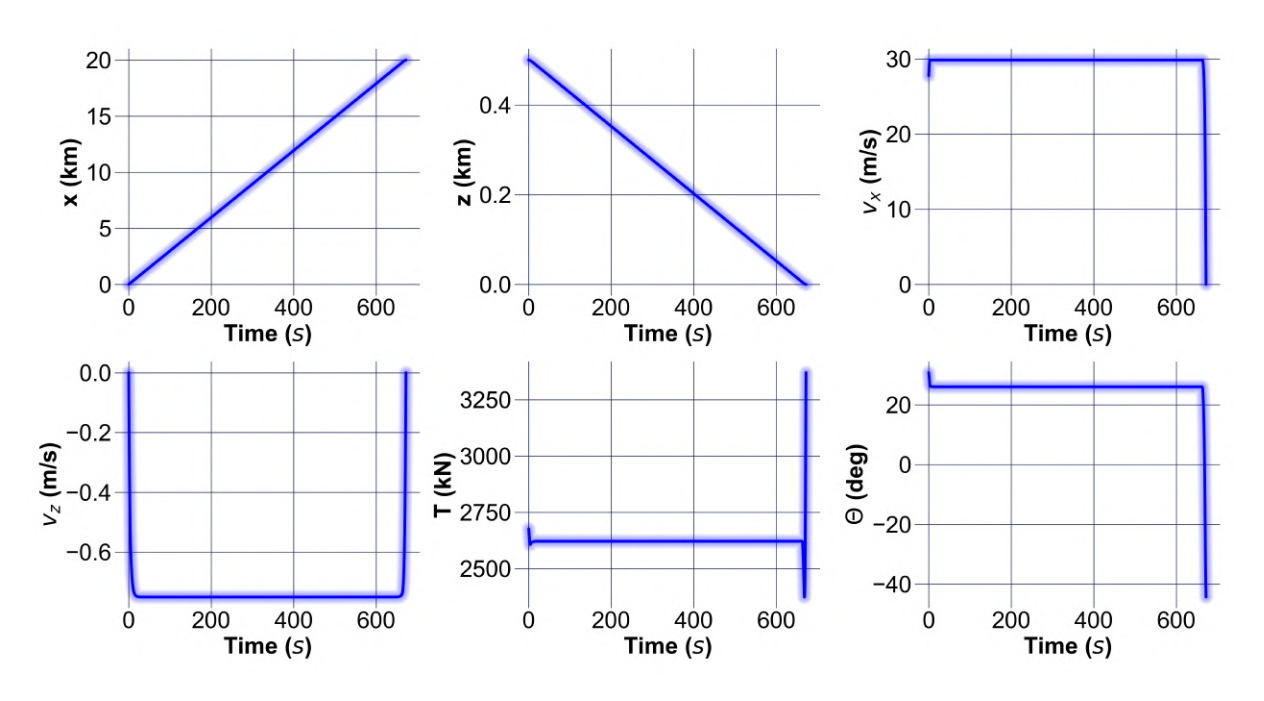


Figure 7 – States and control time histories for case 3 are shown in this figure. There are sharp changes at the start and end of the controls and velocities, making this case quite hard to solve.

eVTOL vehicle increases. Like the other two cases, sharp changes in velocities are present, thereby

resulting in ill-conditioned matrices. These matrices make the problem quite difficult to solve.

While running the continuation process on v_{MAX} , its value is brought down at the expense of an increased time of flight. This is shown in Fig. 8, where the red dashed line is the seed solution and the blue solid line is the final trajectory.

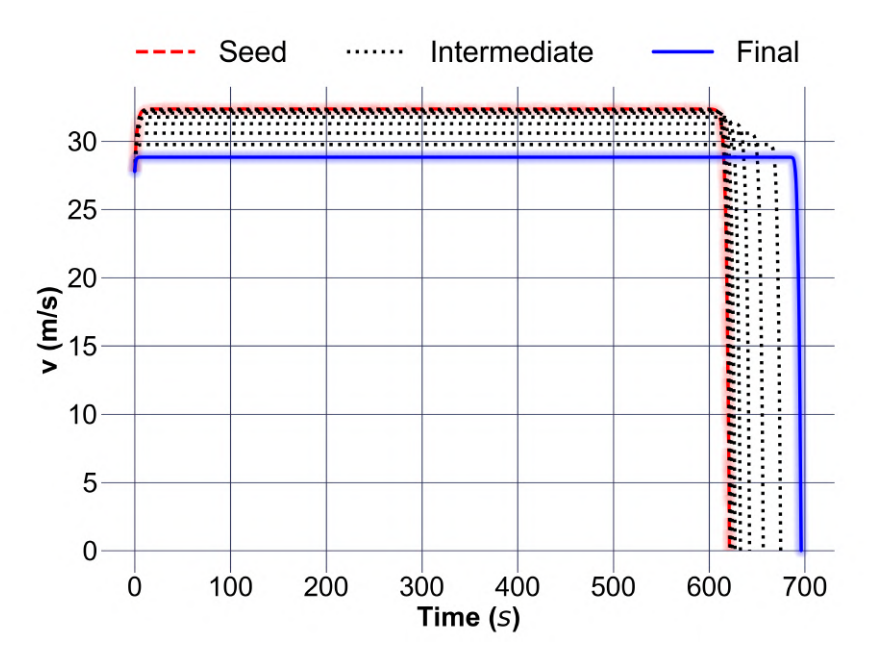


Figure 8 – Results for continuation on v_{MAX} are shown in this plot. Red dashed line indicates the results without any constraint on v_{MAX} . The intermediate results are shown in black dotted lines. The final trajectory with v_{MAX} as 30 m/s is shown in blue solid line.

Similarly, Fig. 9 depicts the continuation process on ε_{ν} , which results in a decreased time of flight. As the value of ε_{ν} is reduced, the solution gets closer to the upper bound on ν . Thus, the velocity starts reaching its upper bound, thereby requiring lesser time to reach the final states.

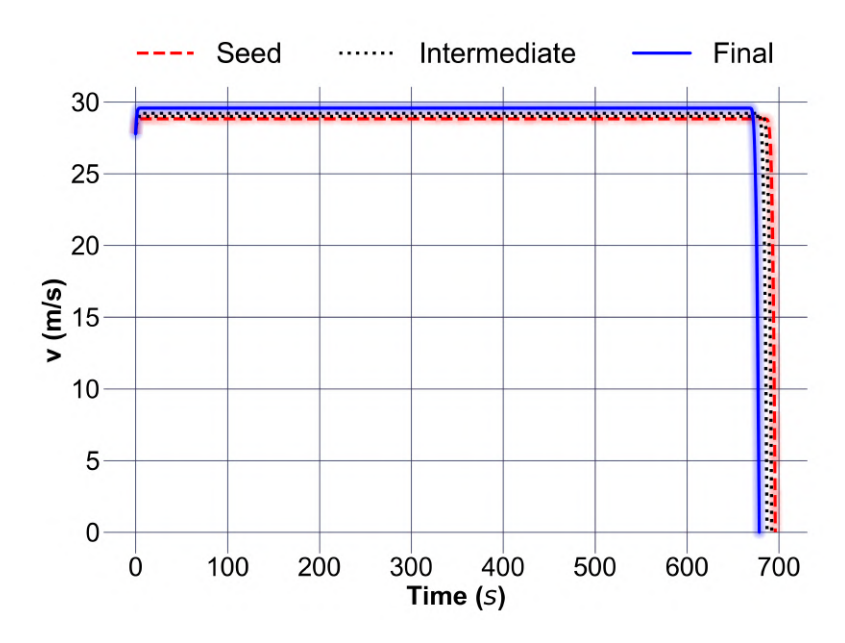


Figure 9 – This plot shows the results for continuation on ε_{ν} . The red dashed line indicates the results for ε_{ν} as 10^{-4} . The intermediate results are shown in black dotted lines. The final trajectory with ε_{ν} as 10^{-8} is shown in a blue solid line.

The impact of ε_{ν} was also analyzed on the value of the objective functional, J, and is shown in Fig. 10. It was found that reducing ε_{ν} beyond a certain value was not useful in obtaining more optimal J values. Thus, for this study, the final value of ε_{ν} was chosen as 10^{-8} .

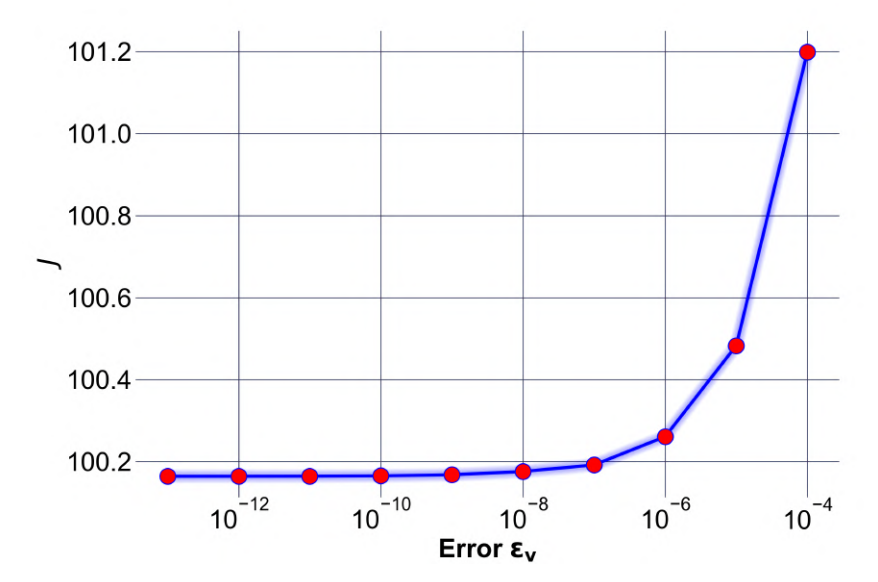


Figure 10 – Objective J is shown as a function of error ε_{ν} in this plot. Below a certain error value, the objective value does not improve and only adds to the computation time. Thus, a value of 10^{-8} for ε_{ν} is sufficient for this case.

4.4 Results Comparison

The results obtained for the three cases are summarized in Table 8. Note that the objective values in this table were calculated from the thrust data using the trapz function given by

$$J^* = \operatorname{trapz}\left(t, \frac{1}{2} \left(\frac{T}{T_{\mathsf{MAX}}}\right)^2\right). \tag{8}$$

Table 8 – Comparison between the three cases of the UAM trajectory optimization problem.

	Computation Time (s)	Trajectories (#)	Objective (s)	Time of Flight (s)	ν _{ΜΑΧ} (m/s)
Case 1	5	55	99.314	619.9	32.43
Case 2	4	195	182.169	1,500	27.78
Case 3	62	262	100.170	669.5	29.98

4.5 Advantages and Limitations of the Uniform Trigonometrization Method

The UTM generates analytical and closed-form expressions for the control law and the costate dynamics after placing implicit bounds on the controls and states. Several useful parameter sweeps related to the eVTOL vehicle can be easily and quickly done using the numerical continuation process of the UTM. The continuation plots lead to additional useful insights regarding the structure of trajectories. Moreover, the UTM guarantees locally optimal trajectories.

Though the UTM has several advantages over traditional indirect methods, its main drawback is the expertise required for its setup. Engineering intuition and thus experience, with some degree of trial and error, are required right now to establish the continuation process used in the UTM. The work of Nolan [46] made some notable progress in this regard, and furthering this line of work seems justified to widen the applicability of UTM-based approaches.

5. Conclusions and Future Work

This study aimed at finding optimal trajectories of electric vertical take-off and landing (eVTOL) vehicles for urban air mobility (UAM). An advance indirect method of optimization, the Uniform Trigonometrization Method (UTM), was used to generate these optimal trajectories. Three cases with different constraints on the time of flight and maximum velocity of the eVTOL vehicle were solved. This study concludes that the UTM can be very effective in solving complex trajectory optimization problems pertaining to UAM missions. When the time of flight is constrained and forced to be large, the eVTOL vehicle flies on a safer trajectory even without constraining velocity. If the time of flight is left free, the safety and comfort of the passengers can be ensured through a constraint on the maximum velocity. The UTM guarantees locally optimal trajectories, which ensures the results obtained are of high resolution. The results obtained for this study using the UTM matched those obtained using a direct pesudospectral method-based solver, GPOPS-II. This study showcases that additional insights can be gained through the numerical continuation process utilized in the UTM.

Future work includes automatic determination of the sequence and step size of each continuation set in the numerical continuation process of the UTM. More complex versions of the eVTOL trajectory optimization problem for UAM missions are yet to be solved. These problems involve more complex dynamics and objective functionals, including the state of charge of the vehicle.

6. Contact Author Email Address

mailto: mall@purdue.edu

7. Copyright Statement

The authors confirm that they, and/or their company or organization, hold copyright on all of the original material included in this paper. The authors also confirm that they have obtained permission, from the copyright holder of any third party material included in this paper, to publish it as part of their paper. The authors confirm that they give permission, or have obtained permission from the copyright holder of this paper, for the publication and distribution of this paper as part of the ICAS proceedings or as individual off-prints from the proceedings.

References

- [1] Adam P Cohen, Susan A Shaheen, and Emily M Farrar. Urban air mobility: History, ecosystem, market potential, and challenges. *IEEE Transactions on Intelligent Transportation Systems*, 22(9):6074–6087, 2021.
- [2] M. Naga Praveen Babu, Sidvik Basa, Prasanth Kumar Duba, and P. Rajalakshmi. Future mobility with evtol personal air vehicle (pav): Urban air mobility (uam) concept. In *International Conference on Electrical and Electronics Engineering (ICEEE 2022)*, pages 323–337, 2022.
- [3] Yasir Mahmood Khan, Mehmet Efe Balli, and Lorenzo Trainelli. Generic evtol aircraft preliminary sizing method for aam/uam missions. In 48th European Rotorcraft Forum (ERF 2022), pages 1–8, 2022.
- [4] Nicholas I. Gunady, Seejay R. Patel, and Daniel Delaurentis. A System-of-Systems Approach to Analyzing Future Advanced Air Mobility Cargo Operations. In *2022 17th Annual System of Systems Engineering Conference, SOSE 2022*, pages 368–373. Institute of Electrical and Electronics Engineers Inc., 2022.
- [5] Nicholas I. Gunady, Spruha Vashi, Byeonghun Kim, Hsun Chao, Daniel A DeLaurentis, and William A Crossley. Exploring middle mile cargo operations with urban air mobility across metro areas. In AIAA Aviation 2023 Forum, 2023.
- [6] Brandon E. Sells, Keshav Iyengar, Byeonghun Kim, Nicholas I. Gunady, Ethan Wright, Seejay R. Patel, Daniel A. DeLaurentis, and William A. Crossley. A Comparative Study of Operational Limits for Urban and Regional Passenger-Carrying Missions across Metropolitans. In *AIAA Aviation 2023 Forum*. American Institute of Aeronautics and Astronautics (AIAA), 6 2023.
- [7] Seejay R. Patel, Nicholas I. Gunady, Akshay K. Rao, Ethan C. Wright, and Daniel Delaurentis. Modeling Energy Infrastructure of Future Electric Urban Air Mobility Operations. In 2022 17th Annual System of Systems Engineering Conference, SOSE 2022, pages 382–387. Institute of Electrical and Electronics Engineers Inc., 2022.

TRAJECTORY OPTIMIZATION OF EVTOL VEHICLES FOR UAM

- [8] Apoorv Maheshwari, Sai Mudumba, Brandon E Sells, Daniel A DeLaurentis, and William A Crossley. Identifying and analyzing operations limits for passenger-carrying urban air mobility missions. In *AIAA Aviation 2020 Forum*, page 2913, 2020.
- [9] Adler Edsel, Somrick Das Biswas, Rishikesh Gadre, Spruha Vashi, Michael Kilbourne, Kshitij Mall, Daniel A. DeLaurentis, and William Crossley. Exploring ridesharing in passenger urban air mobility: A comparative analysis. In *ICAS 2024*. ICAS, 2024. Accepted.
- [10] Somrick Das Biswas, Adler Edsel, Rishikesh Gadre, Michael Kilbourne, Spruha Vashi, Kshitij Mall, Daniel A. DeLaurentis, and William Crossley. Passenger aggregation network with very efficient listing (PANVEL) ride-sharing model for advanced air mobility. In AIAA Aviation 2024 Forum. AIAA, 2024. Accepted.
- [11] Spruha Vashi, Adler Edsel, Somrick Das Biswas, Gareth Morgan, Michael Kilbourne, Rishikesh Gadre, Kshitij Mall, Daniel A. DeLaurentis, and William Crossley. Refined analysis of co₂ emissions in urban air mobility networks. In AIAA Aviation 2024 Forum. AIAA, 2024. Accepted.
- [12] Celia Fernandez. This city has the worst traffic in the u.s.—and it's actually a good thing: 'congestion shows the economy is moving'. *CNBC-Make It*, 2023.
- [13] Xuxi Yang and Peng Wei. Autonomous free flight operations in urban air mobility with computational guidance and collision avoidance. *IEEE Transactions on Intelligent transportation systems*, 22(9):5962–5975, 2021.
- [14] Jin Park, Inrae Kim, Jinyoung Suk, and Seungkeun Kim. Trajectory optimization for takeoff and landing phase of uam considering energy and safety. In *Aerospace Science and Technology*, volume 140, 2023.
- [15] Yufei Wu, Sabrullah Deniz, and Zhenbo Wang. A convex approach to high-fidelity landing trajectory optimization for advanced air mobility. In *AIAA SCITECH 2024 Forum*, 2024.
- [16] Kshitij Mall and Michael James Grant. Epsilon-Trig Regularization Method for Bang-Bang Optimal Control Problems. *Journal of Optimization Theory and Applications*, 174(2):500–517, 2017.
- [17] Kshitij Mall. Advancing Optimal Control Theory Using Trigonometry For Solving Complex Aerospace Problems. PhD thesis, Purdue University West Lafayette, 2018.
- [18] Kshitij Mall, Michael J Grant, and Ehsan Taheri. Uniform trigonometrization method for optimal control problems with control and state constraints. *Journal of Spacecraft and Rockets*, 57(5):995–1007, 2020.
- [19] Kshitij Mall, Sean M Nolan, and Daniel A DeLaurentis. Solving mixed state-control constraint problems using uniform trigonometrization method. In *AIAA Scitech 2021 Forum*, page 1067, 2021.
- [20] Thomas Antony. Large Scale Constrained Trajectory Optimization Using Indirect Methods. PhD thesis, Purdue University, 2018.
- [21] Thomas Antony and Michael J Grant. Path constraint regularization in optimal control problems using saturation functions. In 2018 AIAA Atmospheric Flight Mechanics Conference, page 0018, 2018.
- [22] Kshitij Mall, Sean M Nolan, Winston C Levin, Lauren Risany, and Daniel A DeLaurentis. Using uniform trigonometrization method for aviation based optimal control problems. In *AIAA Aviation 2023 Forum*, page 3912, 2023.
- [23] Kshitij Mall and Michael J Grant. Trigonometrization of optimal control problems with mixed constraints and linear controls. In *AIAA Scitech 2019 Forum*, page 0261, 2019.
- [24] Kshitij Mall and Michael J Grant. High Mass Mars Exploration Using Slender Entry Vehicles. In *AIAA Atmospheric Flight Mechanics Conference*, page 0019, 2016.
- [25] Janav P Udani, Kshitij Mall, Michael J Grant, and Dengfeng Sun. Optimal flight trajectory to minimize noise during landing. In *55th AIAA Aerospace Sciences Meeting*, page 1180, 2017.
- [26] Joseph Williams, Kshitij Mall, and Michael J Grant. Trajectory optimization using indirect methods and parametric scramjet cycle analysis. In *55th AIAA Aerospace Sciences Meeting*, page 1384, 2017.
- [27] Kshitij Mall and Ehsan Taheri. Optimal control of wave energy converters using epsilon-trig regularization method. In 2020 American Control Conference (ACC), pages 1773–1778. IEEE, 2020.
- [28] Kshitij Mall and Ehsan Taheri. Entry trajectory optimization for mars science laboratory class missions using indirect uniform trigonometrization method. In *2020 American Control Conference (ACC)*, pages 4182–4187. IEEE, 2020.
- [29] Kshitij Mall and Ehsan Taheri. Unified trigonometrization method for solving optimal control problems in atmospheric flight mechanics. In *AIAA Scitech 2020 Forum*, page 0022, 2020.
- [30] Kshitij Mall and Ehsan Taheri. Three-degree-of-freedom hypersonic reentry trajectory optimization using an advanced indirect method. *Journal of Spacecraft and Rockets*, 59(5):1463–1474, 2022.
- [31] Hsun Chao, Sai Mudumba, Kshitij Mall, and Daniel A DeLaurentis. Flight trajectory planning with safe landing assurance under contingent event. In *AIAA SCITECH 2023 Forum*, page 1332, 2023.
- [32] Priyank Pradeep, Gano B Chatterji, Todd A Lauderdale, Kapil Sheth, Chok Fung Lai, Heinz Erzberger, and

TRAJECTORY OPTIMIZATION OF EVTOL VEHICLES FOR UAM

- Banavar Sridhar. Wind-optimal lateral trajectories for a multirotor aircraft in urban air mobility. *Frontiers in Aerospace Engineering*, 1:1064142, 2022.
- [33] Yufei Wu, Sabrullah Deniz, Yang Shi, and Zhenbo Wang. A convex optimization approach to real-time merging control of evtol vehicles for future urban air mobility. In *AIAA Aviation 2022 Forum*, page 3319, 2022.
- [34] Kyowon Song. Optimal vertiport airspace and approach control strategy for urban air mobility (uam). Sustainability, 15(1):437, 2022.
- [35] Weihong Yuan. Optimal Flight Trajectory Generation Algorithms for Urban Air Mobility. PhD thesis, Concordia University, 2020.
- [36] Zhenbo Wang, Peng Wei, and Liang Sun. Optimal cruise, descent, and landing of evtol vehicles for urban air mobility using convex optimization. In *AIAA Scitech 2021 Forum*, page 0577, 2021.
- [37] Michael A Patterson and Anil V Rao. GPOPS-II: A MATLAB Software for Solving Multiple-Phase Optimal Control Problems Using hp-Adaptive Gaussian Quadrature Collocation Methods and Sparse Nonlinear Programming. *ACM Transactions on Mathematical Software (TOMS)*, 41(1):1, 2014.
- [38] Joby Aviation. Joby receives part 135 certification from the faa. Online, 5 2022. Accessed: June 13, 2024.
- [39] Archer Aviation. Archer completes midnight's transition flight, midnight is archer's second full-scale evtol aircraft to achieve this milestone. Online, 6 2024. Accessed: June 13, 2024.
- [40] Lilium Air Mobility. Lilium jet to take flight in the french riviera in 2026. Online, 5 2024. Accessed: June 13, 2024.
- [41] Guangzhou EHang Intelligent Technology Co. Ltd. Ehang showcases eh216 series and vt-30 pilotless evtol aircraft at driftx, eh216-s completes debut flight in abu dhabi. Online, 4 2024. Accessed: June 13, 2024.
- [42] Ben Cooper. Ehang's autonomous helicopter promises to fly you anywhere, no pilot required. *The Verge*, 2016.
- [43] Michael J Grant and Robert D Braun. Rapid Indirect Trajectory Optimization for Conceptual Design of Hypersonic Missions. *Journal of Spacecraft and Rockets*, 52(1):177–182, 2014.
- [44] John L Junkins and Ehsan Taheri. Exploration of Alternative State Vector Choices for Low-Thrust Trajectory Optimizations. *Journal of Guidance, Control, and Dynamics*, 42(1):47–64, 2018.
- [45] James M Longuski, José J Guzmán, and John E Prussing. *Optimal control with aerospace applications*, volume 32. Springer, 2014.
- [46] Sean Matthew Nolan. *Practical Numerical Trajectory Optimization Via Indirect Methods*. PhD thesis, Purdue University, 2023.